Chapter 4
Advanced Topics on Plastic Analysis

4.1 Introduction

This chapter addresses two topics related to the plastic analysis of structures: the first concerns the determination of the collapse load factor under consideration of the interaction effect between internal forces on the plastic capacity of the cross section, and the second concerns the determination of the global displacements and associated deformations of the structure at incipient collapse.

4.2 Plastic Analysis of Structures under N-M Interaction

We study first the problem of the determination of the collapse load factor under consideration of the interaction effect between internal forces on the plastic capacity of the cross section.

4.2.1 Plastic Capacity of Section under Axial Force-Bending Moment Interaction

In this section we establish the effect of the interaction between normal force N and bending moment M on the response of sections under linear elastic, perfectly plastic material response. To this end we establish first the *yield surface*, which describes the initiation of yielding of a cross section under combinations of normal force and bending moment. We then proceed to set up the limit surface of the section under combinations of normal force and bending moment with the assumption of a fully plastic stress state. This surface is also called *plastic N-M interaction surface*.

We limit the following discussion to uniaxial bending with normal force for bi-symmetric sections, but the derivation is completely analogous for biaxial bending with normal force of bi-symmetric and other types of cross sections. Similar considerations can be made for other internal forces such as shear and torsion, in which case a *failure criterion* under the biaxial or triaxial stress state consisting of normal and shear stresses is required. The reader is referred to Chapter 3 of [2] for a concise presentation of the plastic limit surface of steel sections under biaxial bending, and for the plastic limit surface under the interaction of bending moment and shear force.

4.2.1.1 Rectangular Section

First, we establish the combination of axial N and bending moment M corresponding to the initiation of yielding for a cross section, i.e. the instant when the highest stress reaches the yield strength f_y of

the material. In the following we derive this relation for a rectangular section and show that the final result holds for any type of bi-symmetric cross section.

Under the assumption that plane sections remain plane the normal strain distribution over the section is always linear. Fig. 4.1 shows the strain and stress distribution over a rectangular cross section with depth d and width b under a normal force N and a bending moment M. Both internal forces are depicted in the positive direction in the figure. The stress distribution in Fig. 4.1 is depicted at the instant that the largest strain reaches the yield strain ε_y.

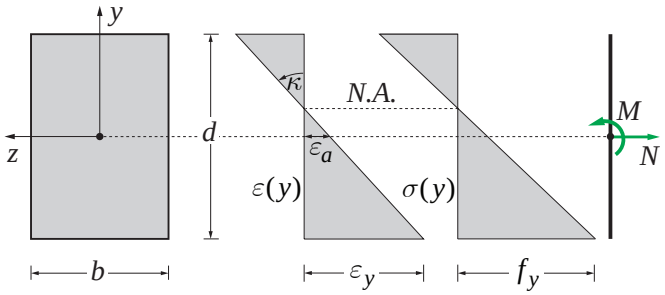

Fig. 4.1: Stress state for rectangular cross section under axial force N and bending moment M at yield initiations

Consequently, the stress distribution is linear for linear elastic, perfectly plastic material response. Using the coordinate system y-z with origin the centroid of the cross section the stress $\sigma(y)$ at a distance y from the centroid is

$$\sigma(y) = \frac{N}{A} - \frac{My}{I}$$

noting that a positive moment causes a compressive stress for positive y. For the case in Fig. 4.1 with the highest stress reaching the yield strength f_y of the material we set $y = -d/2$ and $\sigma = f_y$ to get

$$f_y = \frac{N}{A} + \frac{M\frac{d}{2}}{I} = \frac{N}{A} + \frac{M\frac{d}{2}}{\frac{bd^3}{12}} = \frac{N}{A} + \frac{M}{\frac{bd^2}{6}} = \frac{N}{A} + \frac{M}{S}$$

where $S = \frac{I}{d/2} = \frac{bd^2}{6}$ is the elastic section modulus. While the latter expression holds only for a rectangular section, the former is general as is the final form of the preceding equation

$$f_y = \frac{N}{A} + \frac{M}{S}$$

which holds for any bi-symmetric cross section. Dividing both sides of the last equation by f_y gives

$$1 = \frac{N}{Af_y} + \frac{M}{Sf_y} = \frac{N}{N_y} + \frac{M}{M_y}$$

where Af_y is the axial force N_y at the yield initiation under normal force only, and Sf_y is the moment M_y at the yield initiation under bending moment only according to (1.4). Noting that N_y is equal to the plastic axial capacity N_p in (1.1), while the yield moment M_y is related to the plastic moment capacity M_p through the shape factor α of the cross section, and considering all combinations of axial force $\pm N$ with bending moment $\pm M$ gives

$$\frac{|N|}{N_y} + \frac{|M|}{M_y} = 1 \quad \rightarrow \quad \frac{|N|}{N_y} + \alpha\frac{|M|}{M_p} = 1 \quad \text{with} \quad \alpha = \frac{M_p}{M_y} \tag{4.1}$$

The combinations of N and M satisfying (4.1) constitute the elastic limit surface of the cross section.

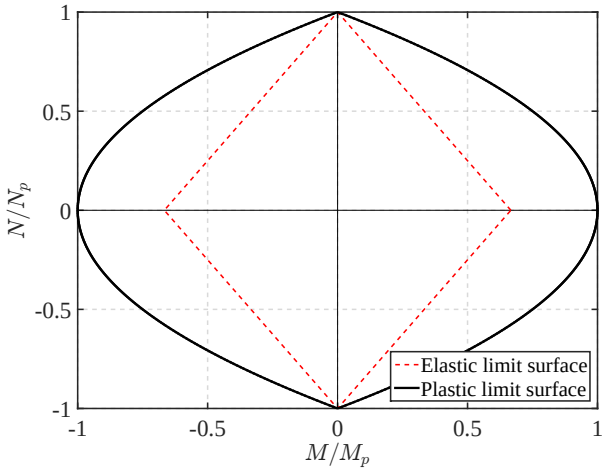

Fig. 4.2: Elastic and plastic limit surface of rectangular section

We use the term surface so as to account for the general case of more than two variables, but for the case in hand with only two variables the combinations of N and M satisfying (4.1) represent 4 lines in the N-M plane in Fig. 4.2 bounding a diamond-shaped area that corresponds to combinations of N and M within the linear elastic range of material response. This linear elastic range is represented by the inequality

$$\frac{|N|}{N_y} + \alpha \frac{|M|}{M_p} \leq 1$$

where $\alpha = 1.5$ for the rectangular section, as discussed in Chapter 1. Combinations of N and M that fall outside the diamond shaped area in Fig. 4.2 give rise to nonlinear material response.

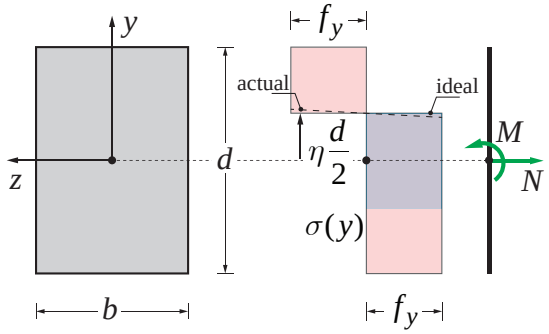

Fig. 4.3: Fully plastic stress state for rectangular cross section under axial force N and bending moment M

We are interested now in establishing the combinations of N and M corresponding to the plastic capacity of the cross section. In this case the material reaches its yield strength over most of the cross section under a very large curvature. Even though, a small portion of the section remains within the elastic range, as Fig. 4.3 shows, we idealize the stress distribution by two rectangular stress blocks, one under the tensile yield strength f_y and the other under the compressive yield strength $-f_y$. This ideal stress state of Fig. 4.3 is attainable for a linear elastic, perfectly plastic material only in the limit as the curvature of the cross section approaches infinity, as was discussed in Chapter 1 in connection with (1.8).

In the presence of a normal force N and a bending moment M the neutral axis is no longer located at the section centroid, so that the difference between the tension stress block and the compression stress block makes up the normal force N.

The fully plastic stress distribution in Fig. 4.3 can be decomposed in two parts that are symmetric about the centroid of the cross section. The first part consists of the stress block with height ηd in Fig. 4.3 that extends symmetrically relative to the centroid and thus does not contribute to the bending moment resistance, while the second part consists of the outer tensile stress block and the compressive stress block with equal resultant force that does not contribute to the normal force. We can, therefore, sum up the stresses of the inner block to establish the corresponding normal force N, and sum up the moment of the resultant force pair for the outer stress blocks to obtain the bending moment M. For the rectangular section of depth d and width b in Fig. 4.3 this gives

$$N = f_y\,[b(\eta d)] = \eta N_p$$
$$M = f_y\,2\left[b(1-\eta)\frac{d}{2}\right]\frac{1}{2}(1+\eta)\frac{d}{2} = f_y\frac{bd^2}{4}(1-\eta^2) = M_p(1-\eta^2)$$

where $N_p = Af_y$ and $M_p = Zf_y$ with $A = bd$ and $Z = \frac{bd^2}{4}$. Solving for the depth ratio η of the contiguous stress block in Fig. 4.3 and substituting the result into the equation for the bending moment M gives

$$\frac{M}{M_p} = \left[1 - \left(\frac{N}{N_p}\right)^2\right]$$

Moving the internal forces to the same side of the equation sign as the bending moment and accounting for a positive or negative moment gives

$$\left(\frac{N}{N_p}\right)^2 + \frac{|M|}{M_p} = 1 \tag{4.2}$$

(4.2) represents the fully plastic limit surface of a rectangular section. For the case in hand with only two internal forces as variables, it is a curve in the plane with coordinate axes of $x = \frac{M}{M_p}$ and $y = \frac{N}{N_p}$, as Fig. 4.2 shows. Combinations of N and M that fall outside the plastic limit surface exceed the plastic capacity of the cross section and *are not feasible* under perfectly plastic material response. Consequently, the plastic limit surface constitutes a *bounding surface* for all feasible N-M combinations, which satisfy the inequality

$$\left(\frac{N}{N_p}\right)^2 + \frac{|M|}{M_p} \leq 1 \tag{4.3}$$

(4.3) thus represents *the plastic condition* of the cross section to be used for the collapse load determination under the interaction of the axial force N with the bending moment M.

4.2.1.2 Wide Flange Section

The elastic limit surface of a wide flange section with linear elastic, perfectly plastic material is given by (4.1), which holds for any bi-symmetric cross section. For wide flange shapes bent about the strong axis, α ranges from 1.1 for lighter beam sections to 1.23 for heavier column sections.

The plastic limit surface for a wide flange section about the strong axis of bending can be established by subtracting the plastic limit surface of a rectangle of width $b_f - b_w$ and depth $d - 2t_f$ from the plastic limit surface of a rectangle of width b_f and depth d, where b_f is the flange width, b_w the web thickness, t_f the flange thickness, and d the section depth (idealized section).

Fig. 4.4 shows the elastic and the plastic limit surface for a light W10x26 and a heavy W14x426 section about the strong axis of bending. It is clear from Fig. 4.4 that the plastic limit surface of a wide flange section resembles the diamond shape of the elastic limit surface. In fact, in the limit case of a section with shape factor α equal to 1, the plastic limit surface is perfectly diamond shaped, since it coincides with the elastic limit surface. Such an ideal section results from two flanges with area equal to half of the cross section area A at distance d from each other, where d is the section depth. Lighter W-sections with a higher proportion of the total area concentrated in the flange with a shape factor of approximately 1.1 approximate this case, as Fig. 4.4(a) shows for the W10x26 shape. Heavier W-sections suitable for columns with a shape factor around 1.2 have a plastic limit surface in between that of the rectangular section and the diamond shape of an ideal two flange section, as Fig. 4.4(b) shows for the W14x426 shape. In contrast, wide flange sections bent about the weak axis of bending have a plastic limit surface with a shape closer to that of the rectangular section.

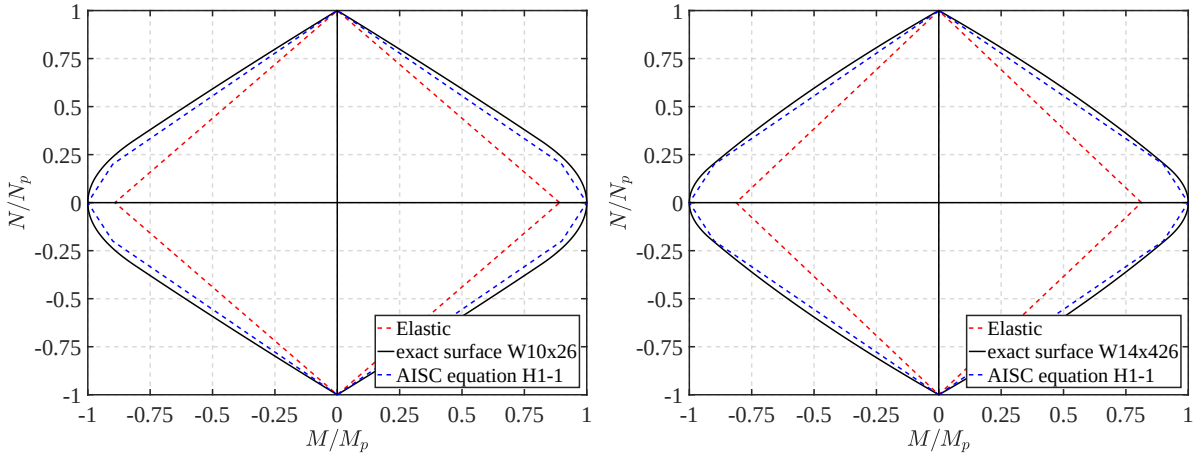

(a) Limit Surfaces and AISC Approximation for W10x26 (b) Limit Surfaces and AISC Approximation for W14x426

Fig. 4.4: Plastic and elastic limit surfaces of two wide flange section and corresponding polygonal AISC approximation

For first and second order plastic analysis under consideration of the interaction between axial force and bending moment a simple polygonal approximation of the plastic limit surface of a wide-flange section suggests itself. This approach is used in design specifications, such as the 2005 AISC specification that is a more accurate evolution of the earlier formula in the ASCE Manual 41 on "Plastic Design in Steel" (1971). The interaction relation for steel beam-columns under uniaxial bending and normal force is given by equation H1-1 of the 2005 AISC specification

$$\begin{aligned} &\text{for } \frac{P_r}{P_c} \geq 0.2 \qquad \frac{P_r}{P_c} + \frac{8}{9}\frac{M_r}{M_c} \leq 1 \\ &\text{for } \frac{P_r}{P_c} < 0.2 \qquad \frac{P_r}{2P_c} + \frac{M_r}{M_c} \leq 1 \end{aligned} \tag{4.4}$$

For the definition of terms in the above equations consult Section H1.1 of the 2005 AISC Specification. Fig. 4.4 shows the elastic and the plastic limit surface and compares the latter with the polygonal approximation of the 2005 AISC Specification for a light W10x26 and a heavy W14x426 section. The figures show that the AISC Specification approximates the exact surface very well and is slightly conservative by lying inside.

4.2.2 Plastic Conditions for Structural Elements

In order to account for the interaction between the axial force N and the bending moment M in the determination of the collapse load factor λ_c of structural models by the lower bound theorem of plastic analysis we need to modify the plastic conditions for the basic forces of the frame element in (2.7) and (2.8).

To clarify the form of the plastic conditions we write (2.8) explicitly in the form of (2.10) after substituting (2.7) for $\boldsymbol{q}_{pl}^{+}$ and $\boldsymbol{q}_{pl}^{-}$

$$\begin{matrix} \boldsymbol{q} \leq \boldsymbol{q}_{pl}^{+} \\ -\boldsymbol{q} \leq \boldsymbol{q}_{pl}^{+} \end{matrix} \quad \rightarrow \quad \begin{pmatrix} \boldsymbol{q}_1 \\ \boldsymbol{q}_2 \\ \boldsymbol{q}_3 \\ -\boldsymbol{q}_1 \\ -\boldsymbol{q}_2 \\ -\boldsymbol{q}_3 \end{pmatrix} \leq \begin{pmatrix} N_p^+ \\ M_p^- \\ M_p^+ \\ N_p^- \\ M_p^+ \\ M_p^- \end{pmatrix} \quad \rightarrow \quad \begin{pmatrix} \boldsymbol{q}_1/N_p^+ \\ \boldsymbol{q}_2/M_p^- \\ \boldsymbol{q}_3/M_p^+ \\ -\boldsymbol{q}_1/N_p^- \\ -\boldsymbol{q}_2/M_p^+ \\ -\boldsymbol{q}_3/M_p^- \end{pmatrix} \leq \begin{pmatrix} 1 \\ 1 \\ 1 \\ 1 \\ 1 \\ 1 \end{pmatrix} \tag{4.5}$$

The last relation results by dividing each basic element force by the corresponding plastic capacity and accounting for the general case that the positive and negative capacities may be different. The lack of an interaction between N and M is reflected in the fact that the plastic condition of each basic element force is checked independently noting that $\boldsymbol{q}_1 = N$, $\boldsymbol{q}_2 = -M_i$ and $\boldsymbol{q}_3 = M_j$ with i and j denoting the element ends.

For the linear programming implementation we express the last relation in (4.5) in the following form

$$\begin{bmatrix} \frac{1}{N_p^+} & 0 & 0 \\ 0 & \frac{1}{M_p^-} & 0 \\ 0 & 0 & \frac{1}{M_p^+} \\ -\frac{1}{N_p^-} & 0 & 0 \\ 0 & -\frac{1}{M_p^+} & 0 \\ 0 & 0 & -\frac{1}{M_p^-} \end{bmatrix} \begin{pmatrix} \boldsymbol{q}_1 \\ \boldsymbol{q}_2 \\ \boldsymbol{q}_3 \end{pmatrix} \leq \begin{pmatrix} 1 \\ 1 \\ 1 \\ 1 \\ 1 \\ 1 \end{pmatrix} \tag{4.6}$$

which clearly isolates the basic element forces $\boldsymbol{q}$ as problem unknowns. Collecting the inequalities in (4.6) for all elements of the structural model involves stacking the basic element forces $\boldsymbol{q}$ to form $\boldsymbol{Q}$ and collecting the coefficient matrix of each element in (4.6) in block diagonal form to generate the inequalities in (2.11) or (2.12) in slightly modified form.

We account for the interaction between the axial force N and the bending moment M at the end sections of a frame element where the bending moments are largest or smallest in the absence of element loading. In order to use linear programming methods for the determination of the collapse load factor by the lower bound theorem of plastic analysis *we convert the plastic limit surface of the end sections into a convex polygon*, as was the case in the AISC Specification for steel beam columns with (4.4).

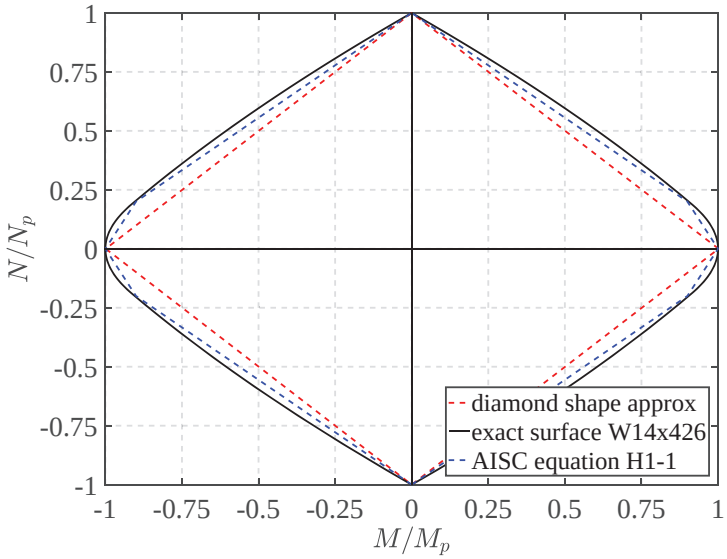

Fig. 4.5: Plastic limit surface of W14x426 wide flange section and two convex polygon approximations

Fig. 4.5 shows the plastic limit surface for the W14x426 wide flange section and two convex polygon approximations:

1) The first approximation uses the linear relation for the elastic limit surface in (4.1); setting $\alpha = 1$ stretches the surface along the M-axis so that the surface intersects is at $M = M_p$.

2) The second approximation follows (4.4) which is rewritten here in terms of N, N_p and M, M_p

$$\begin{aligned} &\text{for } \frac{N}{N_p} \geq 0.2 \qquad && \frac{N}{N_p} + \frac{8}{9}\frac{M}{Mp} \leq 1 \\ &\text{for } \frac{N}{N_p} < 0.2 \qquad && \frac{N}{2N_p} + \frac{M}{M_p} \leq 1 \end{aligned} \tag{4.7}$$

Fig. 4.5 shows that the first approximation is slightly more conservative, but also easier to implement requiring 4 inequalities at each end for a total of 8, instead of the 6 inequalities for the case with no interaction in (4.6). In contrast, the AISC approximation of the plastic limit surface requires 8 inequalities at each end for a total of 16 thus doubling the number of inequalities for the frame elements with N-M interaction.

We modify the inequalities in (4.6) to account for the N-M interaction with the first approximation of the plastic limit surface. Substituting (4.1) with $\alpha = 1$ in (4.6) and noting that $\boldsymbol{q}_1 = N$, $\boldsymbol{q}_2 = -M_i$ and $\boldsymbol{q}_3 = M_j$ gives

$$\left[\begin{array}{ccc} \frac{1}{N_p^+} & \frac{1}{M_{pi}^-} & 0 \\ -\frac{1}{N_p^-} & \frac{1}{M_{pi}^-} & 0 \\ \frac{1}{N_p^+} & -\frac{1}{M_{pi}^+} & 0 \\ -\frac{1}{N_p^-} & -\frac{1}{M_{pi}^+} & 0 \\ \hline \frac{1}{N_p^+} & 0 & \frac{1}{M_{pj}^+} \\ -\frac{1}{N_p^-} & 0 & \frac{1}{M_{pj}^+} \\ \frac{1}{N_p^+} & 0 & -\frac{1}{M_{pj}^-} \\ -\frac{1}{N_p^-} & 0 & -\frac{1}{M_{pj}^-} \end{array}\right] \begin{pmatrix} \boldsymbol{q}_1 \\ \boldsymbol{q}_2 \\ \boldsymbol{q}_3 \end{pmatrix} \leq \begin{pmatrix} 1 \\ 1 \\ 1 \\ 1 \\ 1 \\ 1 \end{pmatrix} \tag{4.8}$$

where we generalized the inequalities by assuming that the plastic moment capacities at end j may not be the same as the capacities at end i. In the opposite case, the terms of the third column are the same as the corresponding terms of the second. The horizontal line in the coefficient matrix separates the 4 inequalities at end i from those at end j.

In similar fashion we can express the 16 inequalities for the AISC approximation of the plastic limit surface in (4.7). This is left as an exercise for the reader.

In conclusion,

The approximation of the plastic limit surface by a convex polygon renders the plastic conditions linear, so that the linear programming methods of the lower and the upper bound theorem of plastic analysis can be used for the determination of the collapse load factor of a structural model under N-M interaction.

4.2.3 Examples

Example 4.1 Cantilever Column

We determine the collapse load factor for the cantilever column of height L under two cases of loading (a) and (b) in Fig. 4.6(a). In the first case the gravity load P_v is applied first and held constant while the lateral load P_h is increased by load factor λ until reaching the plastic capacity of the section at the base. In the second case the gravity load P_v and the lateral load P_h are increased simultaneously by the same load factor λ until reaching the plastic capacity of the section at the base.

We approximate the plastic limit surface of the section at the base by the diamond shaped surface in Fig. 4.6(b) with the following equation

$$\frac{|N|}{N_p} + \frac{|M|}{M_p} = 1 \tag{4.9}$$

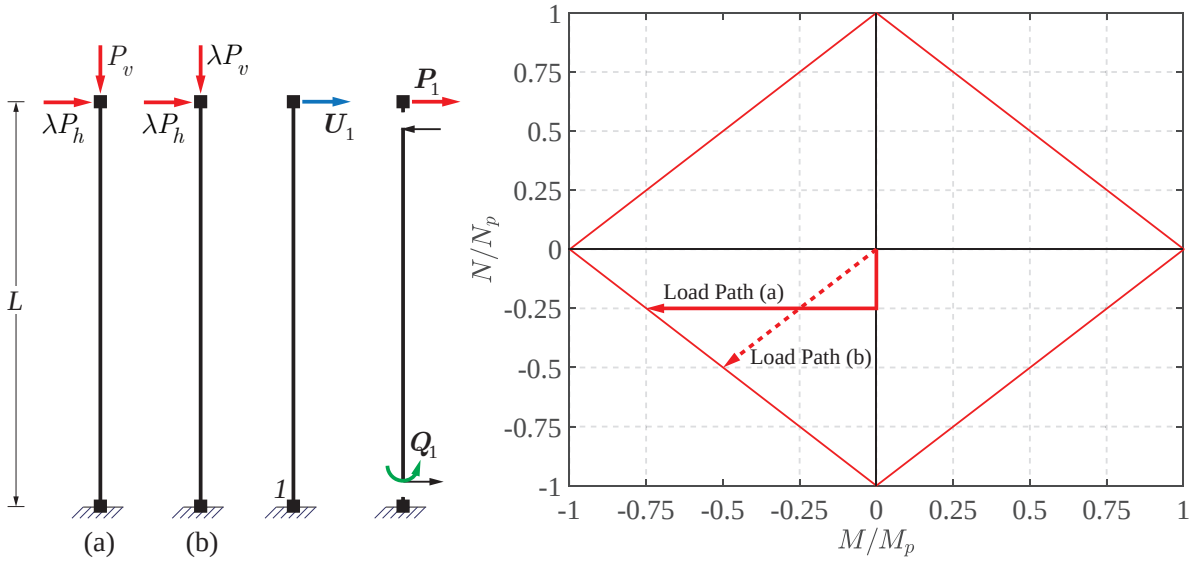

(a) Geometry and load cases

(b) Diamond shaped interaction surface

Fig. 4.6: Cantilever column under two load paths to collapse

For load case (a) $N = -P_v$ and $M = -\lambda P_h L$. Substituting these into (4.9) gives

$$\frac{P_v}{N_p} + \lambda_c \frac{P_h L}{M_p} = 1 \quad \rightarrow \quad \lambda_c = \left(\frac{1 - \frac{P_v}{N_p}}{P_h L} \right) M_p$$

Assuming $\frac{P_v}{N_p} = 0.25$ gives the load path (a) in Fig. 4.6(b) with a bending moment M at the base equal to $-0.75 M_p$ at collapse.

For load case (b) $N = -\lambda P_v$ and $M = -\lambda P_h L$. Substituting these into (4.9) gives

$$\lambda_c \frac{P_v}{N_p} + \lambda_c \frac{P_h L}{M_p} = 1 \quad \rightarrow \quad \lambda_c = \left(\frac{1}{P_v \frac{Z}{A} + P_h L} \right) M_p$$

where Z is the plastic section modulus and A is the area of the base section. The load path to collapse and the collapse load factor depends on the values of P_v and P_h as well as the ratio Z/A and the height L of the column. Fig. 4.6(b) shows the load path to collapse for load case (b) for the case that

$$P_v \frac{Z}{A} + P_h L = 2$$

4.3 Deformation State at Incipient Collapse

4.3.1 Introduction

An important application of the relations governing the response of a linear elastic, structure that is either statically determinate or statically indeterminate with a small degree of static indeterminacy,

is the determination of the deformation state of a structural model at incipient collapse. *If the collapse mechanism of a structure is complete, the structure is statically determinate and stable just before the last hinge forms.* Consequently, the deformation-force relations for statically determinate structures in B-Chapter 8 can be used to determine the free dof displacements and deformations of the structure at incipient collapse, including the plastic deformations at all plastic hinges before the last.

If the collapse mechanism of a structure is partial, the structure is statically indeterminate and stable just before the last hinge forms. Because the basic forces $\boldsymbol{Q}$ are known at the plastic hinge locations, the degree of static indeterminacy of the structure is rather small relative to the large number of global degrees of freedom. Consequently, the force method of analysis is the most suitable approach for determining the basic forces at incipient collapse, especially for small structural models.

It is assumed that the number and location of the plastic hinges under the collapse load factor λ_c are known from the application of the upper bound theorem of plastic analysis.

If the number of plastic hinges is such that a unique static solution for the basic forces $\boldsymbol{Q}_c$ results, then the structure is statically determinate at incipient collapse. In this case, the strain-dependent element deformations $\boldsymbol{V}_\varepsilon$ can be established in all elements. Just before the last hinge forms, the structure is stable and the number of unknown free dof displacements matches the number of available kinematic relations. It is, therefore, possible to determine the free dof displacements and plastic hinge deformations at incipient collapse from the basic forces $\boldsymbol{Q}_c$ and the corresponding element deformations $\boldsymbol{V}_\varepsilon$ just as for any statically determinate structure.

There is one problem, however: *we need to know where the last hinge forms.* Clearly, we can use a step-by-step analysis that determines the sequence of plastic hinge formation to answer the question of which is the last plastic hinge to form, but the expense of this process is not proportional to the objective of just determining the deformation state at incipient collapse. A direct method for accomplishing this task is, therefore, required, as discussed in the next section.

4.3.2 Solution Process

The solution process for determining the last plastic hinge to form before the structure becomes a mechanism is based on the following assumptions:

1) The applied loading consists only of the reference load $\boldsymbol{P}_{ref}$, which is increased monotonically by incrementing the load factor λ until reaching the collapse load factor λ_c.
2) Plastic hinges that are "open" under a load factor λ cannot "close" under a higher load factor: this means that plastic hinge deformations increase monotonically under the monotonically increasing reference load.

Given these conditions we can determine the location of the last plastic hinge to form by making a guess and then correcting it, as described in the following process.

Before starting the process for the determination of the last hinge to form it is assumed that the following tasks are complete:

1) The upper or lower bound theorem of plastic analysis gives the collapse load factor λ_c and the plastic hinge locations for the collapse mechanism.

2) The equilibrium equations give a unique solution for the basic forces $\boldsymbol{Q}_c$ at incipient collapse, because of the complete collapse mode of the structure.
3) The element deformation-force relations give the element deformations $\boldsymbol{V}_\varepsilon$ at incipient collapse

$$\boldsymbol{V}_\varepsilon = \mathbf{F}_s \boldsymbol{Q}_c + \boldsymbol{V}_0$$

The process for the determination of the last hinge to form consists of the following steps:

1) Select any hinge of the collapse mechanism as last to form and solve the kinematic relations for the corresponding free dof displacements $\boldsymbol{U}_f^{tr}$, where the superscript *tr* stands for *trial result*.
2) Determine the plastic hinge deformations $\boldsymbol{V}_{hp}^{tr}$ corresponding to $\boldsymbol{U}_f^{tr}$ with

$$\boldsymbol{V} = \boldsymbol{V}_\varepsilon + \boldsymbol{V}_{hp}^{tr} = \mathbf{A}_f \boldsymbol{U}_f^{tr}$$

3) If the sign of each plastic deformation matches the sign of the corresponding basic force $\boldsymbol{Q}_c$ from the equilibrium equations, the last hinge location is correct. The trial displacements and plastic deformations from steps (1) and (2) give the free dof displacements $\boldsymbol{U}_f$ and the plastic deformations $\boldsymbol{V}_{hp}$ at incipient collapse.
4) If the sign of one or more plastic deformations does not match the sign of the corresponding basic force, *correct the free dof displacements and plastic deformations* of Step (1) and (2) in a single step as described in the following.

If the sign of one or more plastic deformations does not match the sign of the corresponding basic force, the assumption about the last plastic hinge location in Step (1) is not correct. Consequently, the free dof displacements and plastic deformations of Steps (1) and (2) need to be corrected. The correction involves the addition of the deformation state of the collapse mechanism of the structure. The independent dof of the collapse mechanism is scaled so that *the total plastic deformations match everywhere the sign of the corresponding basic force, except for one location where the plastic deformation is zero, thus, identifying the location of the last plastic hinge to form.*

The determination of the scale factor for the collapse mechanism is described next. Consider the initial assumption about the deformation state of the structure at incipient collapse. The kinematic relations give

$$\boldsymbol{V}_\varepsilon + \boldsymbol{V}_{hp}^{tr} = \mathbf{A}_f \boldsymbol{U}_f^{tr} \tag{4.10}$$

From the comparison of the sign of the plastic deformations $\boldsymbol{V}_{hp}^{tr}$ with the sign of the corresponding basic forces $\boldsymbol{Q}_c$ we identify n locations of mismatch. We need to correct these plastic deformations by adding a deformation state *without changing the element deformations* $\boldsymbol{V}_\varepsilon$. Because $\Delta\boldsymbol{V}_\varepsilon$ is zero during the collapse mechanism displacement, we conclude that we need to superimpose to the deformation state in (4.10) the deformation state of the collapse mechanism with a single independent dof $\dot{U}_p$. For this deformation state it holds that

$$\Delta\boldsymbol{V}_{hp} = \mathbf{A}_{mp}\, \Delta U_p \tag{4.11}$$

where we have converted instantaneous rates of change to increments denoted with a Δ prefix for the corresponding variable. Consequently, ΔU_p is the displacement increment of the single independent dof of the collapse mechanism and $\Delta\boldsymbol{V}_{hp}$ are the increments of the corresponding plastic deformations.

Because of the principle of maximum plastic dissipation, the non-zero entries of the kinematic vector $\mathbf{A}_{mp}$ of the collapse mechanism match the sign of the corresponding basic force at the plastic hinge. Consequently, *the addition of* (4.11) *to* (4.10) *corrects the plastic deformations with mismatched signs.*

The displacement increment ΔU_p of the independent dof of the collapse mechanism is determined so as to close the most critical plastic hinge among the n plastic hinges with sign mismatch. From the condition

$$\boldsymbol{V}_{hp_k}^{tr} + \Delta \boldsymbol{V}_{hp_k} = 0 \;\rightarrow\; \boldsymbol{V}_{hp_k}^{tr} + \mathbf{A}_{mp_k}\, \Delta U_p = 0 \tag{4.12}$$

for a location k among the n locations with sign mismatch, we conclude that the independent dof displacement increment ΔU_p of the collapse mechanism is

$$\Delta U_p = \max \left[\frac{-\boldsymbol{V}_{hp_k}^{tr}}{\mathbf{A}_{mp_k}} \right] \quad \text{among all } k \in n \tag{4.13}$$

Once the value of ΔU_p is determined from (4.13) the displacements at incipient collapse can be determined from the superposition of the trial displacements $\boldsymbol{U}_f^{tr}$ with the free dof displacements of the collapse mechanism scaled by ΔU_p. We get

$$\boldsymbol{U}_f = \boldsymbol{U}_f^{tr} + \mathbf{A}_{cp}\, \Delta U_p \tag{4.14}$$

The same is true for the plastic deformations at incipient collapse, namely

$$\boldsymbol{V}_{hp} = \boldsymbol{V}_{hp}^{tr} + \mathbf{A}_{mp}\, \Delta U_p \tag{4.15}$$

An alternative and more direct way of determining the plastic deformations at incipient collapse can be established from the kinematic relations

$$\boldsymbol{V} = \boldsymbol{V}_\varepsilon + \boldsymbol{V}_{hp} = \mathbf{A}_f \boldsymbol{U}_f$$

Solving for $\boldsymbol{V}_{hp}$ gives the following relation

$$\boldsymbol{V}_{hp} = \mathbf{A}_f \boldsymbol{U}_f - \boldsymbol{V}_\varepsilon \tag{4.16}$$

Note: We use the kinematic matrix $\mathbf{A}_f$ in the preceding relations and not $\breve{\mathbf{A}}_f$ because the element deformations are originally continuous at the plastic hinge locations.

4.3.3 Displacements and Deformations Beyond Incipient Collapse

Once the collapse mechanism initiates with the formation of the last hinge the free dof displacement and plastic deformation increments are described by the collapse mechanism kinematics. If the target displacement at a particular dof m is given by displacement ductility requirements or other performance-based criteria, then the displacement increment ΔU_p^* of the single independent dof of the collapse mechanism can be determined from the condition

$$\boldsymbol{U}^*_{f_m} = \boldsymbol{U}_{f_m} + \mathbf{A}_{cp_m}\, \Delta U^*_p \tag{4.17}$$

where $*$ denotes the variables of the target deformation state with $\boldsymbol{U}^*_{f_m}$ the target displacement at a particular dof m of the structure. $\boldsymbol{U}_{f_m}$ denotes the displacement at incipient collapse and $\mathbf{A}_{cp_m}$ the displacement of the collapse mechanism at dof m.

After determining ΔU^*_p from (4.17) the free dof displacements and plastic deformations at the target deformation state are

$$\begin{aligned} \boldsymbol{U}^*_f &= \boldsymbol{U}_f + \mathbf{A}_{cp}\, \Delta U^*_p \\ \boldsymbol{V}^*_{hp} &= \mathbf{A}_f\, \boldsymbol{U}^*_f - \boldsymbol{V}_\varepsilon \end{aligned} \tag{4.18}$$

with $\boldsymbol{U}_f$ denoting the free dof displacements at incipient collapse and $*$ denoting the variables of the target deformation state.

4.3.4 Examples

The following examples demonstrate the process of determining the last plastic hinge to form with a wrong initial guess and the correction procedure of the preceding section followed by the subsequent determination of the free dof displacements and plastic deformations at incipient collapse.

Example 4.2 Simple Truss

(a) Uniform Axial Stiffness EA

The determination of the collapse load factor λ_c and the basic forces at incipient collapse $\boldsymbol{Q}_c$ of the simple truss in Fig. 4.7 were discussed in Example 2.1.

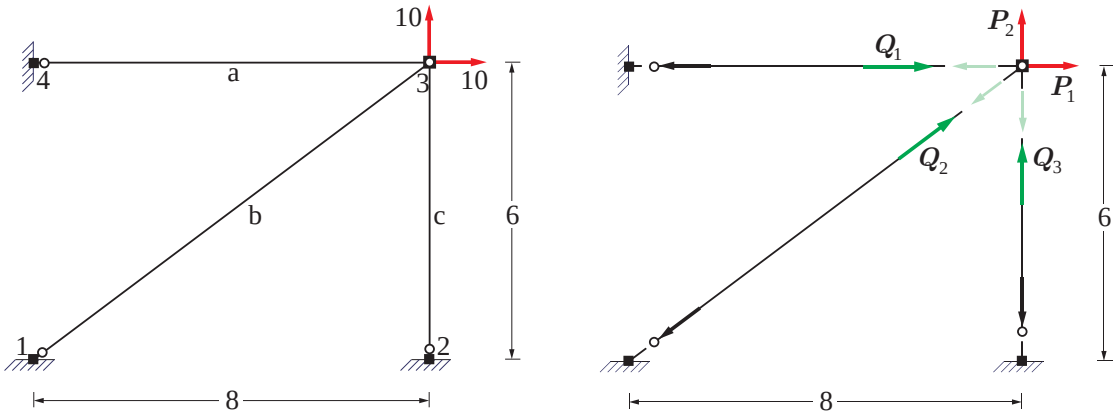

(a) Geometry and loading (b) Free dof equation and basic force numbering

Fig. 4.7: Geometry, loading, equilibrium equation and basic force numbering for truss model of B-Example **??**

Recalling the equilibrium equations

$$\begin{aligned} \lambda(10) &= \boldsymbol{Q}_1 + 0.8\boldsymbol{Q}_2 \\ \lambda(10) &= \quad 0.6\boldsymbol{Q}_2 + \boldsymbol{Q}_3 \end{aligned}$$

the collapse load factor λ_c under the reference forces of Fig. 4.7(a) is 2.4 and the basic forces $\boldsymbol{Q}_c$ at incipient collapse are $\boldsymbol{Q}_1 = 12$, $\boldsymbol{Q}_2 = 15$, $\boldsymbol{Q}_3 = 15$ with plastic hinges forming in elements b and c.

If the truss elements have the same axial stiffness EA, the element deformations $\boldsymbol{V}_\varepsilon$ are

$$\begin{aligned}(EA)\,\boldsymbol{V}_{\varepsilon_1} &= L_a\boldsymbol{Q}_1 \;= 96\\ (EA)\,\boldsymbol{V}_{\varepsilon_2} &= L_b\boldsymbol{Q}_2 = 150\\ (EA)\,\boldsymbol{V}_{\varepsilon_3} &= L_c\boldsymbol{Q}_3 \;= 90\end{aligned}$$

The kinematic relations are

$$\begin{aligned}\boldsymbol{V}_1 &= \quad \boldsymbol{U}_1\\ \boldsymbol{V}_2 &= 0.8\boldsymbol{U}_1 + 0.6\boldsymbol{U}_2\\ \boldsymbol{V}_3 &= \qquad\quad \boldsymbol{U}_2\end{aligned} \tag{4.19}$$

With hinges forming in elements b and c the kinematic relations of the collapse mechanism are

$$\begin{aligned}\dot{\boldsymbol{V}}_{\varepsilon_1} &= \quad \dot{\boldsymbol{U}}_1\\ \dot{\boldsymbol{V}}_{\varepsilon_2}+\dot{\boldsymbol{V}}_{hp_2} &= 0.8\dot{\boldsymbol{U}}_1 + 0.6\dot{\boldsymbol{U}}_2\\ \dot{\boldsymbol{V}}_{\varepsilon_3}+\dot{\boldsymbol{V}}_{hp_3} &= \qquad\quad \dot{\boldsymbol{U}}_2\end{aligned} \tag{4.20}$$

noting that $\dot{\boldsymbol{V}}_\varepsilon = \boldsymbol{0}$ under the collapse mechanism displacement. Setting $\dot{\boldsymbol{V}}_\varepsilon = \boldsymbol{0}$ in (4.20) gives $\dot{\boldsymbol{U}}_1 = 0$. Selecting the translation $\dot{\boldsymbol{U}}_2$ as the single independent dof $\dot{U}_p$ of the collapse mechanism gives

$$\begin{pmatrix}\dot{\boldsymbol{U}}_1\\ \dot{\boldsymbol{U}}_2\end{pmatrix} = \begin{pmatrix}0\\1\end{pmatrix}\dot{U}_c = \mathbf{A}_{cp}\dot{U}_c \quad \text{with} \quad \mathbf{A}_{cp} = \begin{pmatrix}0\\1\end{pmatrix}$$

or, in incremental form

$$\begin{pmatrix}\Delta\boldsymbol{U}_1\\ \Delta\boldsymbol{U}_2\end{pmatrix} = \mathbf{A}_{cp}\,\Delta U_p$$

The plastic deformation rates from (4.20) are

$$\dot{\boldsymbol{V}}_{hp} = \begin{pmatrix}0\\0.6\\1\end{pmatrix}\dot{U}_c = \mathbf{A}_{mp}\dot{U}_c \quad \text{with} \quad \mathbf{A}_{mp} = \begin{pmatrix}0\\0.6\\1\end{pmatrix}$$

or, in incremental form

$$\Delta\boldsymbol{V}_{hp} = \mathbf{A}_{mp}\,\Delta U_p$$

We assume that the last hinge to form is in element c. In this case the hinge in element b has undergone plastic deformation when the truss reaches the state of incipient collapse, whereas no plastic deformation is present in element c, since the plastic hinge is about to form there. We use the first and third kinematic relations in (4.19) to determine the free dof displacements $\boldsymbol{U}_f^{tr}$ at incipient collapse

$$\begin{aligned}(EA)\boldsymbol{U}_1^{tr} &= (EA)\boldsymbol{V}_{\varepsilon_1}\\ (EA)\boldsymbol{U}_2^{tr} &= (EA)\boldsymbol{V}_{\varepsilon_3}\end{aligned} \quad \rightarrow \quad \begin{aligned}(EA)\boldsymbol{U}_1^{tr} &= 96\\ (EA)\boldsymbol{U}_2^{tr} &= 90\end{aligned}$$

With these values we determine the plastic deformation in element b from the second kinematic relation in (4.19)

$$(EA)\boldsymbol{V}_{hp_2}^{tr} = 0.8(96) + 0.6(90) - 150 = -19.2$$

Because the sign of the plastic deformation in element b is inconsistent with the positive sign of the basic force $\boldsymbol{Q}_2$ *in the element, the initial guess for the location of the last hinge to form is wrong and needs to be corrected.*

To correct the plastic hinge deformation in element b we add the deformation state of the collapse mechanism according to (4.12). Since there is only one plastic hinge in this simple example, (4.12) reads

$$(EA)\,\boldsymbol{V}_{hp_2}^{tr} + \mathbf{A}_{mp_2}\,(EA)\,\Delta U_p = 0 \quad \rightarrow \quad (EA)\,\Delta U_p = -\frac{(-19.2)}{0.6} = 32 \tag{4.21}$$

The last equation for ΔU_p in (4.21) corresponds to (4.13) for $k = 2$.

With the scaling of the independent dof of the collapse mechanism from (4.21) we obtain the free dof displacements and plastic deformations of the truss at incipient collapse according to (4.14) and (4.15)

$$(EA)\,\boldsymbol{U}_f = \begin{pmatrix} 96 \\ 90 \end{pmatrix} + \begin{pmatrix} 0 \\ 1 \end{pmatrix} (32) = \begin{pmatrix} 96 \\ 122 \end{pmatrix}$$

$$(EA)\,\boldsymbol{V}_{hp} = \begin{pmatrix} 0 \\ -19.2 \\ 0 \end{pmatrix} + \begin{pmatrix} 0 \\ 0.6 \\ 1 \end{pmatrix} (32) = \begin{pmatrix} 0 \\ 0 \\ 32 \end{pmatrix}$$

We see that the superposition of the collapse mechanism with the correct scale factor to the trial deformation state corresponding to the wrong guess for the last plastic hinge location *closes the plastic hinge at b and opens the plastic hinge in element c.* The last hinge to form is, therefore, in element b. We can confirm the result for the plastic deformations with (4.16)

$$(EA)\boldsymbol{V}_{hp} = \begin{bmatrix} 1 & 0 \\ 0.8 & 0.6 \\ 0 & 1 \end{bmatrix} \begin{pmatrix} 96 \\ 122 \end{pmatrix} - \begin{pmatrix} 96 \\ 150 \\ 90 \end{pmatrix} = \begin{pmatrix} 0 \\ 0 \\ 32 \end{pmatrix}$$

(4.16) is very useful if the free dof displacements at incipient collapse are known from a computer analysis. In such case (4.16) is used for determining or confirming the plastic deformations $\boldsymbol{V}_{hp}$ at incipient collapse.

(b) Effect of Relative Stiffness on Plastic Hinge Formation Sequence

The plastic hinge formation sequence of the simple truss changes with the relative element stiffness.

We can show this for the simple truss by considering the case that the axial stiffness of element b is equal to $2EA$. If the plastic axial capacities remain the same, the collapse load factor λ_c and the basic forces $\boldsymbol{Q}_c$ at collapse *do not change.* Only the element deformation of element b changes to $(EA)\boldsymbol{V}_{\varepsilon_2} = L_b\boldsymbol{Q}_2 = 75$. Assuming that the last hinge to form is in element c gives the same free dof displacement values as before. The plastic deformation in element b now becomes

$$(EA)\boldsymbol{V}_{hp_2}^{tr} = 0.8(96) + 0.6(90) - 75 = 55.8$$

Because the sign of the plastic deformation in element b now matches the sign of the basic force, the initial guess about the last plastic hinge to form is correct. We conclude that element b attracts a larger share of the applied forces with its higher stiffness and yields before element c in this case.

Example 4.3 Propped Cantilever

We determine the collapse load factor λ_c of the propped cantilever with span $2L$ in Fig. 4.8(a) under a vertical force P_v at midspan. The girder elements have plastic flexural capacity M_p.

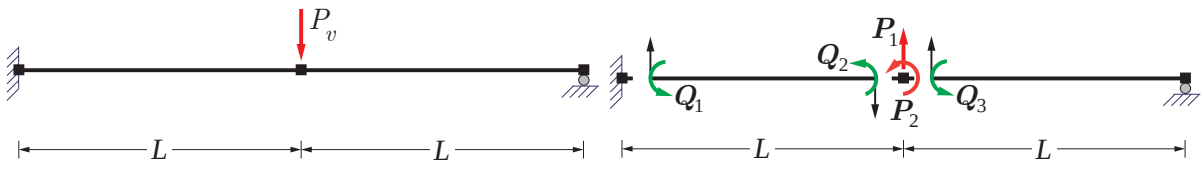

(a) Geometry and loading (b) Free dof equation and basic force numbering

Fig. 4.8: Propped cantilever under vertical force P_v

The equilibrium equations of the structure with the free dof and basic force numbering in Fig. 4.8(b) are

$$\begin{aligned} \boldsymbol{P}_1 &= -\frac{\boldsymbol{Q}_1 + \boldsymbol{Q}_2}{L} + \frac{\boldsymbol{Q}_3}{L} \\ \boldsymbol{P}_2 &= \quad \boldsymbol{Q}_2 + \boldsymbol{Q}_3 \end{aligned}$$

Substituting the given loading under consideration of the load factor λ gives

$$\begin{aligned} \lambda(-P_v) &= -\frac{\boldsymbol{Q}_1 + \boldsymbol{Q}_2}{L} + \frac{\boldsymbol{Q}_3}{L} \\ 0 &= \quad \boldsymbol{Q}_2 + \boldsymbol{Q}_3 \end{aligned} \quad \rightarrow \quad \begin{aligned} \lambda(P_v L) &= \boldsymbol{Q}_1 + \boldsymbol{Q}_2 - \boldsymbol{Q}_3 \\ 0 &= \boldsymbol{Q}_2 + \boldsymbol{Q}_3 \end{aligned} \quad \rightarrow \quad \lambda(P_v L) = \boldsymbol{Q}_1 + 2\boldsymbol{Q}_2$$

It is now clear that the collapse load factor results when $\boldsymbol{Q}_1 = M_p$ and $\boldsymbol{Q}_2 = M_p$ and is

$$\lambda_c = \frac{3M_p}{P_v L}$$

and the basic element forces $\boldsymbol{Q}_c$ at incipient collapse are

$$\boldsymbol{Q}_c = \begin{pmatrix} M_p \\ M_p \\ -M_p \end{pmatrix}$$

Next, we determine the deformation state at incipient collapse. To this end we set up first the kinematic relations for the free dofs and element deformations with the numbering in Fig. 4.9(a)

$$\begin{aligned} \boldsymbol{V}_1 &= -\frac{\boldsymbol{U}_1}{L} \\ \boldsymbol{V}_2 &= -\frac{\boldsymbol{U}_1}{L} + \boldsymbol{U}_2 \\ \boldsymbol{V}_3 &= \quad \frac{\boldsymbol{U}_1}{L} + \boldsymbol{U}_2 \end{aligned}$$

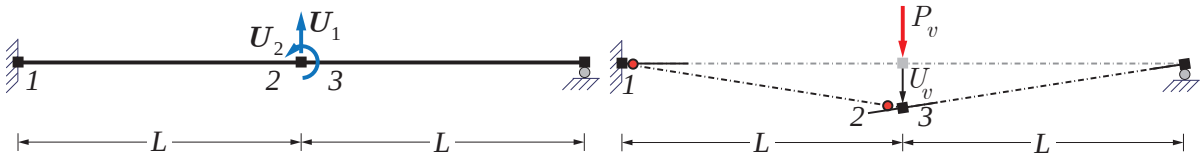

(a) Free dof and deformation numbering (b) Collapse mechanism

Fig. 4.9: Free dof and deformation numbering; collapse mechanism of propped cantilever

With hinges forming at the fixed end and at midspan the kinematic relations at incipient collapse are

$$\begin{aligned} \boldsymbol{V}_{\varepsilon_1} + \boldsymbol{V}_{pl_1} &= -\frac{\boldsymbol{U}_1}{L} \\ \boldsymbol{V}_{\varepsilon_2} + \boldsymbol{V}_{pl_2} &= -\frac{\boldsymbol{U}_1}{L} + \boldsymbol{U}_2 \\ \boldsymbol{V}_{\varepsilon_3} &= \frac{\boldsymbol{U}_1}{L} + \boldsymbol{U}_2 \end{aligned} \tag{4.22}$$

with either $\boldsymbol{V}_{pl_1}$ or $\boldsymbol{V}_{pl_2}$ equal to zero, because the corresponding hinge is only about to form.

The incremental kinematic relations of the collapse mechanism are

$$\begin{aligned} \dot{\boldsymbol{V}}_{\varepsilon_1} + \dot{\boldsymbol{V}}_{pl_1} &= -\frac{\dot{\boldsymbol{U}}_1}{L} \\ \dot{\boldsymbol{V}}_{\varepsilon_2} + \dot{\boldsymbol{V}}_{pl_2} &= -\frac{\dot{\boldsymbol{U}}_1}{L} + \dot{\boldsymbol{U}}_2 \quad \rightarrow \quad 0 = \frac{\dot{\boldsymbol{U}}_1}{L} + \dot{\boldsymbol{U}}_2 \quad \rightarrow \quad \dot{\boldsymbol{U}}_2 = -\frac{\dot{\boldsymbol{U}}_1}{L} \quad \rightarrow \\ \dot{\boldsymbol{V}}_{\varepsilon_3} &= \frac{\dot{\boldsymbol{U}}_1}{L} + \dot{\boldsymbol{U}}_2 \end{aligned} \qquad \begin{aligned} \dot{\boldsymbol{V}}_{pl_1} &= -\frac{\dot{\boldsymbol{U}}_1}{L} \\ \dot{\boldsymbol{V}}_{pl_2} &= -\frac{2\dot{\boldsymbol{U}}_1}{L} \\ \dot{\boldsymbol{V}}_{pl_3} &= 0 \end{aligned}$$

on account of $\dot{\boldsymbol{V}}_\varepsilon = \boldsymbol{0}$. With the selection of $\dot{\boldsymbol{U}}_1$ as the independent dof U_p of the plastic collapse mechanism the vectors $\mathbf{A}_{cp}$ and $\mathbf{A}_{mp}$ become

$$\mathbf{A}_{cp} = \begin{pmatrix} 1 \\ -\frac{1}{L} \end{pmatrix} \qquad \mathbf{A}_{mp} = \begin{pmatrix} -\frac{1}{L} \\ -\frac{2}{L} \\ 0 \end{pmatrix}$$

Fig. 4.9(b) shows the collapse mechanism. To agree with the direction of the applied nodal force P_v the translation U_v at dof 1 is set equal to the negative value of the independent dof U_p. We can easily confirm the collapse load factor with the upper bound theorem of plastic analysis

$$\lambda_c P_v U_v = M_p \left(\frac{U_v}{L}\right) + M_p \left(\frac{2U_v}{L}\right) \quad \rightarrow \quad \lambda_c = \frac{3M_p}{P_v L}$$

Next we determine the strain-dependent element deformations $\boldsymbol{V}_\varepsilon$ with the element force deformation relations

$$\begin{aligned} \begin{pmatrix} \boldsymbol{V}_{\varepsilon_1} \\ \boldsymbol{V}_{\varepsilon_2} \end{pmatrix} &= \frac{L}{6EI} \begin{bmatrix} 2 & -1 \\ -1 & 2 \end{bmatrix} \begin{pmatrix} M_p \\ M_p \end{pmatrix} = \frac{M_p L}{6EI} \begin{pmatrix} 1 \\ 1 \end{pmatrix} \\ \boldsymbol{V}_{\varepsilon_3} &= \frac{L}{3EI}(-M_p) = -\frac{M_p L}{3EI} \end{aligned}$$

so as to use (4.22) to determine the displacements at incipient collapse. At this deformation state the second of the plastic hinges at 1 and 2 is about to form. Because we do not know which one, we need to make an assumption and set the corresponding plastic deformation in (4.22) equal to zero. Here we assume that the plastic hinge at the fixed end is the last to form so that we set $\boldsymbol{V}_{pl_1}^{tr} = 0$ in (4.22). Using the first and third kinematic relations in (4.22) with the superscript tr to denote *trial* values we can readily determine the free dof displacements $\boldsymbol{U}_1^{tr}$ and $\boldsymbol{U}_2^{tr}$

$$\begin{aligned} \boldsymbol{V}_{\varepsilon_1} + 0 &= -\frac{\boldsymbol{U}_1^{tr}}{L} \\ \boldsymbol{V}_{\varepsilon_2} + \boldsymbol{V}_{pl_2} &= -\frac{\boldsymbol{U}_1^{tr}}{L} + \boldsymbol{U}_2^{tr} \\ \boldsymbol{V}_{\varepsilon_3} &= \frac{\boldsymbol{U}_1^{tr}}{L} + \boldsymbol{U}_2^{tr} \end{aligned} \quad \rightarrow \quad \begin{aligned} \boldsymbol{U}_1^{tr} &= -\boldsymbol{V}_{\varepsilon_1} L \\ \boldsymbol{U}_2^{tr} &= \boldsymbol{V}_{\varepsilon_3} - \frac{\boldsymbol{U}_1^{tr}}{L} \end{aligned} \quad \rightarrow \quad \begin{aligned} \boldsymbol{U}_1^{tr} &= -\frac{M_p L}{6EI} L \\ \boldsymbol{U}_2^{tr} &= -\frac{M_p L}{3EI} - \frac{\boldsymbol{U}_1^{tr}}{L} \end{aligned} \tag{4.23}$$

and finally

$$\begin{aligned} \boldsymbol{U}_1^{tr} &= -\frac{M_p L^2}{6EI} \\ \boldsymbol{U}_2^{tr} &= -\frac{M_p L}{6EI} \end{aligned} \tag{4.24}$$

Substituting the free dof displacement values from (4.24) in the second kinematic relation of (4.23) gives the plastic deformation at 2, namely

$$\boldsymbol{V}_{pl_2}^{tr} = -\frac{\boldsymbol{U}_1^{tr}}{L} + \boldsymbol{U}_2^{tr} - \boldsymbol{V}_{\varepsilon_2} = \frac{M_p L}{6EI} - \frac{M_p L}{6EI} - \frac{M_p L}{6EI} = -\frac{M_p L}{6EI}$$

The negative sign of the plastic deformation $\boldsymbol{V}_{pl}$ at 2 contradicts the positive sign of the corresponding basic element force $\boldsymbol{Q}_2$. We, therefore, conclude that the assumption about the location of the last plastic hinge to form is incorrect.

To correct the plastic deformation discrepancy at 2 without affecting the basic element forces and thus strain-dependent element deformations $\boldsymbol{V}_\varepsilon$ we superimpose the deformations of the plastic collapse mechanism. The objective is to eliminate the plastic deformation at 2, while opening the plastic hinge at 1. Because the plastic deformation increments of the collapse mechanism are consistent with the sign of the corresponding basic element forces, the resulting plastic deformation at 1 will be consistent with the sign of $\boldsymbol{Q}_1$. To eliminate the plastic deformation at 2 the plastic deformation increment needs to be equal to

$$\Delta \boldsymbol{V}_{pl_2} = \frac{M_p L}{6EI}$$

and the corresponding displacement increment ΔU_p of the independent dof of the collapse mechanism needs to be equal to

$$\Delta \boldsymbol{V}_{pl_2} = -\frac{2\Delta U_p}{L} \quad \rightarrow \quad \Delta U_p = -\frac{M_p L^2}{12EI}$$

Thus, with the last plastic hinge forming at 2 the midspan translation of the propped cantilever at incipient collapse is

$$\boldsymbol{U}_1 = \boldsymbol{U}_1^{tr} + \Delta \boldsymbol{U}_1 = \boldsymbol{U}_1^{tr} + \Delta U_p = -\frac{M_p L^2}{6EI} - \frac{M_p L^2}{12EI} = -\frac{M_p L^2}{4EI}$$

and the plastic deformation at 1 is

$$\boldsymbol{V}_{pl_1} = -\frac{\boldsymbol{U}_1}{L} - \boldsymbol{V}_{\varepsilon_1} = \frac{M_p L}{4EI} - \frac{M_p L}{6EI} = \frac{M_p L}{12EI}$$

This result can also be obtained from ΔU_p noting that

$$\boldsymbol{V}_{pl_1} = \boldsymbol{V}_{pl_1}^{tr} + \Delta \boldsymbol{V}_{pl_1} = 0 - \frac{\Delta U_p}{L} = \frac{M_p L}{12EI}$$

This completes the determination of the deformation state of the propped cantilever at incipient collapse.

Example 4.4 Portal Frame

The determination of the collapse load factor λ_c and the basic forces at incipient collapse $\boldsymbol{Q}_c$ of the portal frame in Fig. 4.10(a) were the subject of Example 2.3.

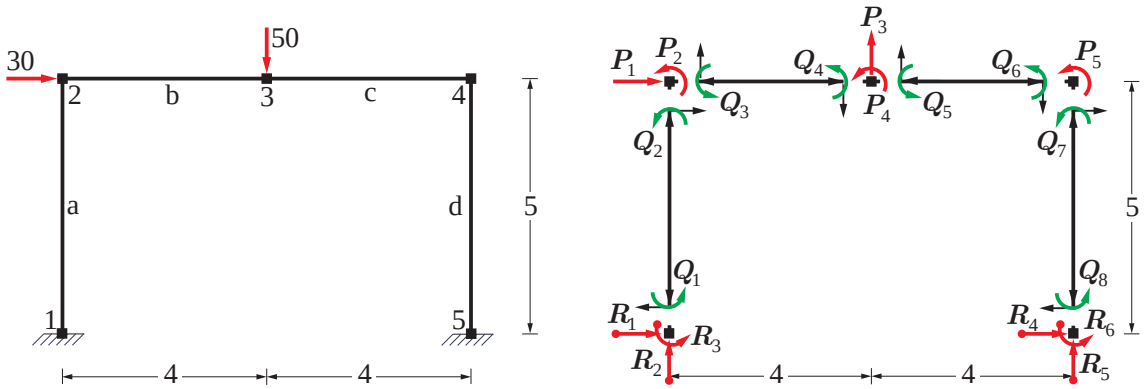

(a) Geometry and loading

(b) Free dof equation and basic force numbering

Fig. 4.10: Portal frame under horizontal and vertical force

Under the given reference values of the nodal forces in Fig. 4.10(a) the collapse load factor is $\lambda_c = 2.229$, the plastic hinges of the collapse mechanism arise at locations 1, 4, 6 and 8, and the basic forces $\boldsymbol{Q}_c$ at incipient collapse are

$$\boldsymbol{Q}_c = \begin{pmatrix} 150 \\ -85.71 \\ 85.71 \\ 120 \\ -120 \\ -120 \\ 120 \\ 150 \end{pmatrix}$$

The bending moment distribution and the corresponding collapse mechanism from Example 2.3 are recalled in Fig. 4.11.

Under the assumption that all elements of the portal frame have the same flexural stiffness EI, the element deformations $\boldsymbol{V}_\varepsilon$ at incipient collapse are

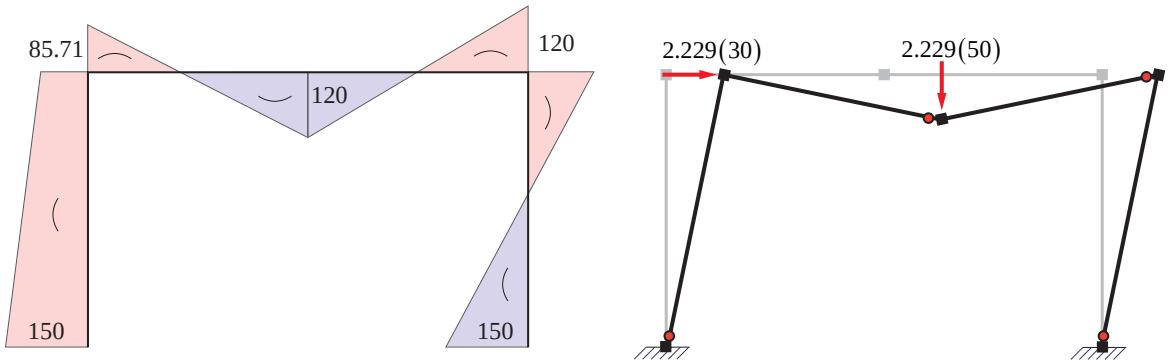

(a) Bending moments at incipient collapse (b) Collapse mode

Fig. 4.11: Bending moments at incipient collapse and collapse mode for portal frame

$$\begin{pmatrix} \boldsymbol{V}_{\varepsilon_1} \\ \boldsymbol{V}_{\varepsilon_2} \end{pmatrix} = \frac{L_a}{6EI} \begin{bmatrix} 2 & -1 \\ -1 & 2 \end{bmatrix} \begin{pmatrix} \boldsymbol{Q}_{c_1} \\ \boldsymbol{Q}_{c_2} \end{pmatrix} = \frac{1}{EI} \begin{pmatrix} 321.4 \\ -267.9 \end{pmatrix}$$
$$\begin{pmatrix} \boldsymbol{V}_{\varepsilon_3} \\ \boldsymbol{V}_{\varepsilon_4} \end{pmatrix} = \frac{L_b}{6EI} \begin{bmatrix} 2 & -1 \\ -1 & 2 \end{bmatrix} \begin{pmatrix} \boldsymbol{Q}_{c_3} \\ \boldsymbol{Q}_{c_4} \end{pmatrix} = \frac{1}{EI} \begin{pmatrix} 34.3 \\ 102.9 \end{pmatrix}$$
$$\begin{pmatrix} \boldsymbol{V}_{\varepsilon_5} \\ \boldsymbol{V}_{\varepsilon_6} \end{pmatrix} = \frac{L_c}{6EI} \begin{bmatrix} 2 & -1 \\ -1 & 2 \end{bmatrix} \begin{pmatrix} \boldsymbol{Q}_{c_5} \\ \boldsymbol{Q}_{c_6} \end{pmatrix} = \frac{1}{EI} \begin{pmatrix} -80 \\ -80 \end{pmatrix}$$
$$\begin{pmatrix} \boldsymbol{V}_{\varepsilon_7} \\ \boldsymbol{V}_{\varepsilon_8} \end{pmatrix} = \frac{L_d}{6EI} \begin{bmatrix} 2 & -1 \\ -1 & 2 \end{bmatrix} \begin{pmatrix} \boldsymbol{Q}_{c_7} \\ \boldsymbol{Q}_{c_8} \end{pmatrix} = \frac{1}{EI} \begin{pmatrix} 75 \\ 150 \end{pmatrix}$$

with $L_a = L_d = 5$ and $L_b = L_c = 4$.

The kinematic relations are

$$\begin{aligned}
\boldsymbol{V}_1 &= \frac{\boldsymbol{U}_1}{5} \\
\boldsymbol{V}_2 &= \frac{\boldsymbol{U}_1}{5} + \boldsymbol{U}_2 \\
\boldsymbol{V}_3 &= \quad + \boldsymbol{U}_2 - \frac{\boldsymbol{U}_3}{4} \\
\boldsymbol{V}_4 &= \qquad - \frac{\boldsymbol{U}_3}{4} + \boldsymbol{U}_4 \\
\boldsymbol{V}_5 &= \qquad + \frac{\boldsymbol{U}_3}{4} + \boldsymbol{U}_4 \\
\boldsymbol{V}_6 &= \qquad + \frac{\boldsymbol{U}_3}{4} \qquad + \boldsymbol{U}_5 \\
\boldsymbol{V}_7 &= \frac{\boldsymbol{U}_1}{5} \qquad\qquad + \boldsymbol{U}_5 \\
\boldsymbol{V}_8 &= \frac{\boldsymbol{U}_1}{5}
\end{aligned}$$

According to Example 3.3 the kinematic relations of the collapse mechanism with plastic hinges at 1, 4, 6 and 8 are

$$
\begin{aligned}
\dot{\boldsymbol{V}}_{\varepsilon_1} + \dot{\boldsymbol{V}}_{hp_1} &= \frac{\dot{\boldsymbol{U}}_1}{5} \\
\dot{\boldsymbol{V}}_{\varepsilon_2} &= \frac{\dot{\boldsymbol{U}}_1}{5} + \dot{\boldsymbol{U}}_2 \\
\dot{\boldsymbol{V}}_{\varepsilon_3} &= + \dot{\boldsymbol{U}}_2 - \frac{\dot{\boldsymbol{U}}_3}{4} \\
\dot{\boldsymbol{V}}_{\varepsilon_4} + \dot{\boldsymbol{V}}_{hp_4} &= - \frac{\dot{\boldsymbol{U}}_3}{4} + \dot{\boldsymbol{U}}_4 \\
\dot{\boldsymbol{V}}_{\varepsilon_5} &= + \frac{\dot{\boldsymbol{U}}_3}{4} + \dot{\boldsymbol{U}}_4 \\
\dot{\boldsymbol{V}}_{\varepsilon_6} + \dot{\boldsymbol{V}}_{hp_6} &= + \frac{\dot{\boldsymbol{U}}_3}{4} + \dot{\boldsymbol{U}}_5 \\
\dot{\boldsymbol{V}}_{\varepsilon_7} &= \frac{\dot{\boldsymbol{U}}_1}{5} + \dot{\boldsymbol{U}}_5 \\
\dot{\boldsymbol{V}}_{\varepsilon_8} + \dot{\boldsymbol{V}}_{hp_8} &= \frac{\dot{\boldsymbol{U}}_1}{5}
\end{aligned}
$$

Setting $\dot{\boldsymbol{V}}_\varepsilon = \boldsymbol{0}$ in the kinematic relations of the collapse mechanism after selecting the translation $\dot{\boldsymbol{U}}_1$ as the single independent dof $\dot{U}_p$ gives according to Example 3.3

$$
\begin{pmatrix} \dot{\boldsymbol{U}}_1 \\ \dot{\boldsymbol{U}}_2 \\ \dot{\boldsymbol{U}}_3 \\ \dot{\boldsymbol{U}}_4 \\ \dot{\boldsymbol{U}}_5 \end{pmatrix} = \begin{pmatrix} 1 \\ -0.2 \\ -0.8 \\ 0.2 \\ -0.2 \end{pmatrix} \dot{U}_{mp} = \mathbf{A}_{cp} \dot{U}_c \quad \text{with} \quad \mathbf{A}_{cp} = \begin{pmatrix} 1 \\ -0.2 \\ -0.8 \\ 0.2 \\ -0.2 \end{pmatrix}
$$

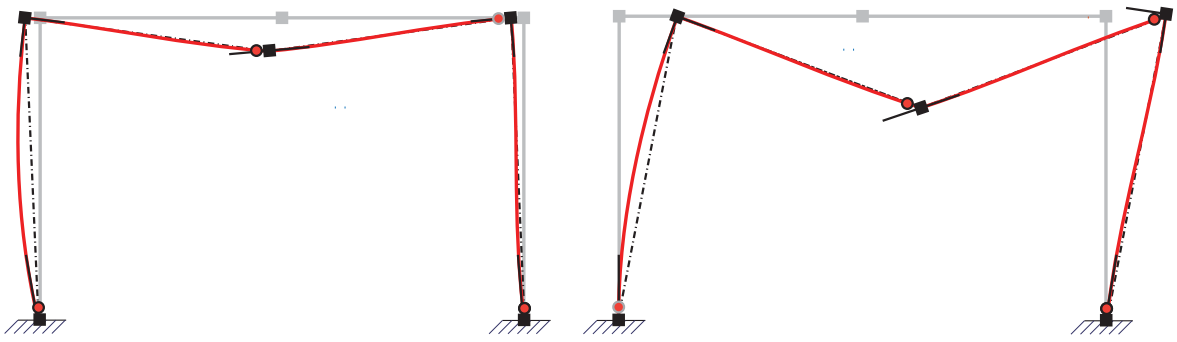

(a) Last hinge to form at $\boldsymbol{V}_6$, i.e. $\boldsymbol{V}_{h_6} = 0$

(b) Last hinge to form at $\boldsymbol{V}_1$, i.e. $\boldsymbol{V}_{h_1} = 0$

Fig. 4.12: Deformed shapes for different guesses of last hinge to form

The plastic deformation rates $\dot{\boldsymbol{V}}_{hp}$ are according to (3.43)

$$
\dot{\boldsymbol{V}}_{hp} = \mathbf{A}_{mp} \dot{U}_p \quad \text{with} \quad \mathbf{A}_{mp} = \begin{bmatrix} 0.2 & 0 & 0 & 0.4 & 0 - 0.4 & 0 & 0.2 \end{bmatrix}^T
$$

We assume that the last hinge forms at end j of element c. In this case $\boldsymbol{V}_{hp_6} = 0$ and we use the kinematic relations 2, 3, 5, 6 and 7 to determine the free dof displacements $\boldsymbol{U}_f^{tr}$ resulting from $\boldsymbol{V}_\varepsilon$. These are

$$\begin{pmatrix} \boldsymbol{U}_1 \\ \boldsymbol{U}_2 \\ \boldsymbol{U}_3 \\ \boldsymbol{U}_4 \\ \boldsymbol{U}_5 \end{pmatrix}^{tr} = \frac{1}{EI} \begin{pmatrix} -367.8 \\ -194.3 \\ -914.3 \\ 148.6 \\ 148.6 \end{pmatrix} \tag{4.25}$$

It is immediately clear that the guess is not correct, because the horizontal translation $\boldsymbol{U}_1$ is to the left, and thus opposite to the applied horizontal force, as shown in Fig. 4.12(a). The last hinge that is about to form at location 6 is depicted with a gray outline.

We proceed to determine the corresponding plastic deformations $\boldsymbol{V}_{hp}^{tr}$ from the kinematic relations $\boldsymbol{V}_{hp} = \mathbf{A}_f \boldsymbol{U}_f - \boldsymbol{V}_\varepsilon$ to get

$$\boldsymbol{V}_{hp}^{tr} = \begin{pmatrix} \boldsymbol{V}_{hp_1} \\ \boldsymbol{V}_{hp_4} \\ \boldsymbol{V}_{hp_6} \\ \boldsymbol{V}_{hp_8} \end{pmatrix}^{tr} = \frac{1}{EI} \begin{pmatrix} -395.0 \\ 274.3 \\ 0 \\ -223.6 \end{pmatrix} \tag{4.26}$$

We conclude that the negative sign for the plastic deformations at 1 and 8 is not consistent with the positive sign of the corresponding basic forces $\boldsymbol{Q}_{c_1}$ and $\boldsymbol{Q}_{c_8}$, respectively. We, therefore, determine the scale factor of the free dof displacement of the collapse mechanism that will correct both inconsistencies. According to (4.13) it is

$$\Delta U_p = \max \left[\frac{-\boldsymbol{V}_{hp_1}^{tr}}{\mathbf{A}_{mp_1}}, \frac{-\boldsymbol{V}_{hp_8}^{tr}}{\mathbf{A}_{mp_8}} \right] = \max \frac{1}{EI} \left[\frac{395}{0.2}, \frac{223.6}{0.2} \right] = \frac{1975}{EI} \tag{4.27}$$

We conclude that the plastic deformation at 1 requires the largest correction and gives the necessary translation increment ΔU_p of the independent free of the collapse mechanism that needs to be added to the free dof displacements in (4.25) to correct the plastic deformation inconsistency for $\boldsymbol{V}_{hp_1}$ and $\boldsymbol{V}_{hp_8}$. With the scaling of the independent dof of the collapse mechanism from (4.27) we obtain the free dof displacements and plastic deformations of the portal frame at incipient collapse with (4.14) and (4.15)

$$\begin{pmatrix} \boldsymbol{U}_1 \\ \boldsymbol{U}_2 \\ \boldsymbol{U}_3 \\ \boldsymbol{U}_4 \\ \boldsymbol{U}_5 \end{pmatrix} = \frac{1}{EI} \begin{pmatrix} -367.8 \\ -194.3 \\ -914.3 \\ 148.6 \\ 148.6 \end{pmatrix} + \frac{1975}{EI} \begin{pmatrix} 1 \\ -0.2 \\ -0.8 \\ 0.2 \\ -0.2 \end{pmatrix} = \frac{1}{EI} \begin{pmatrix} 1607.2 \\ -589.3 \\ -2494.3 \\ 543.6 \\ -246.4 \end{pmatrix}$$

$$\begin{pmatrix} \boldsymbol{V}_{hp_1} \\ \boldsymbol{V}_{hp_4} \\ \boldsymbol{V}_{hp_6} \\ \boldsymbol{V}_{hp_8} \end{pmatrix} = \frac{1}{EI} \begin{pmatrix} -395.0 \\ 274.3 \\ 0 \\ -223.6 \end{pmatrix} + \frac{1975}{EI} \begin{pmatrix} 0.2 \\ 0.4 \\ -0.4 \\ 0.2 \end{pmatrix} = \frac{1}{EI} \begin{pmatrix} 0 \\ 1064.3 \\ -790 \\ 171.4 \end{pmatrix}$$

Fig. 4.12(b) shows the corresponding deformed shape. The last hinge about to form is now at location 1 and is depicted with a gray outline.

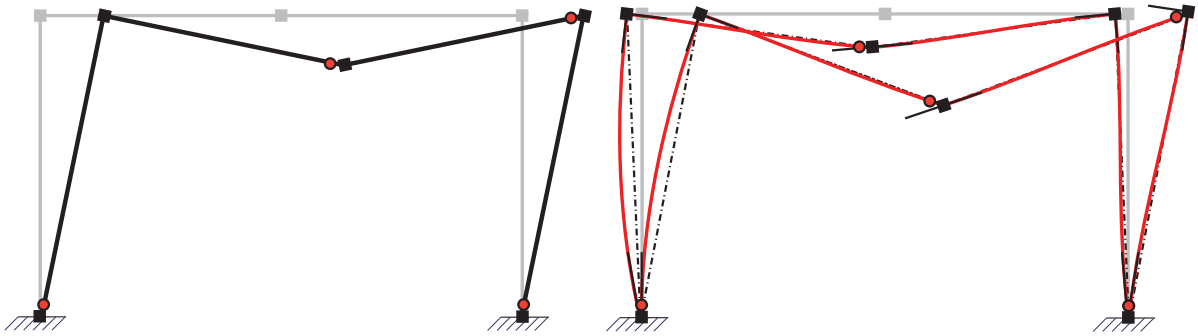

(a) Collapse mechanism (b) Correction from $\boldsymbol{V}_{h_6} = 0$ to $\boldsymbol{V}_{h_1} = 0$

Fig. 4.13: Correction of deformed shape with wrong plastic hinge guess by superposition of collapse mechanism

Fig. 4.13(b) shows that the superposition of the collapse mechanism in Fig. 4.13(a) with the correct scale factor to the trial deformation state corresponding to the wrong guess of the last plastic hinge location *closes the plastic hinge at location 1 and opens one at location 6. It also corrects the plastic deformation at 8, which is now positive and consistent with the sign of the corresponding basic force.* The last hinge to form is, therefore, at the base of the left column at location 1, as confirmed by the vertical tangent to the deformed shape of element a at the left support in Fig. 4.12(b).

Fig. 4.12(b) shows clearly that the addition of the collapse mechanism from Fig. 4.13(a) to the deformed shape for the wrong guess of the last plastic hinge location gives the actual deformed shape at incipient collapse, which is characterized by maximum external work of the applied nodal forces. With the wrong assumption of the last plastic hinge to form at end j of element c the right angle between elements c and d forces the girder of the portal frame to translate to the left giving rise to a negative plastic deformation at the base of column element a, in contradiction with the principle of maximum plastic dissipation. The superposition of the collapse mechanism corrects this discrepancy and closes the hinge at the base of column element a. Because of the single negative curvature of element a, the horizontal translation of the girder is now to the right and both applied nodal forces are performing positive work.

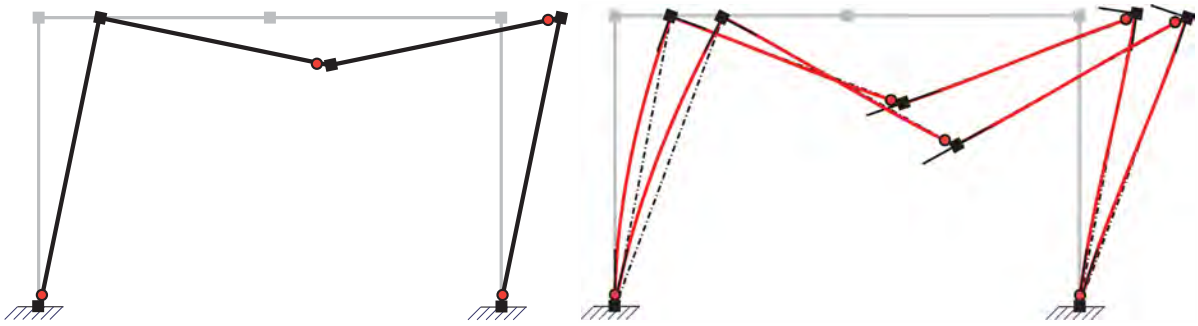

(a) Collapse mechanism (b) Increment from incipient collapse to target translation

Fig. 4.14: Superposition of collapse mechanism to deformed state at incipient collapse to get target horizontal translation

It is worth noting for the deformed shape of the portal frame at incipient collapse in Fig. 4.12(b) that with the exception of element a, which is in single curvature, the deformed shape of the other elements is barely distinguishable from the element chord. The fact that element a is the only one

without plastic deformations further accentuates the deviation of the element deformed shape from the chord. We conclude that the collapse mechanism geometry gives a good approximation of the deformed shape of the portal frame at incipient collapse.

After the formation of the last hinge the structure is transformed into a mechanism with a single independent free dof. As long as the displacements are small relative to the dimensions of the structure, the linear mechanism kinematics of Chapter 3 still hold. For perfectly plastic material response the basic forces $\boldsymbol{Q}_c$ at incipient collapse do not change during the mechanism displacement, so that the increments of the strain-dependent element deformations $\boldsymbol{V}_\varepsilon$ are zero: ($\dot{\boldsymbol{V}}_\varepsilon = \boldsymbol{0}$). Only plastic deformation increments $\dot{\boldsymbol{V}}_{hp}$ occur during the mechanism displacement.

The free dof displacements $\boldsymbol{U}_f^*$ and the plastic deformations $\boldsymbol{V}_{hp}^*$ of the deformation state of the portal frame at any point after the initiation of the collapse mechanism can be determined with (4.18) for a given value of the independent free dof displacement increment ΔU_p^* of the collapse mechanism. The resulting deformed shape of the portal frame for a total horizontal translation of 2% of the height is shown in Fig. 4.14(b) with a magnification factor of 20. Theoretically, an inter-story drift of 2% is large enough that nonlinear geometry effects should be included and we plan to address this issue in a later chapter.

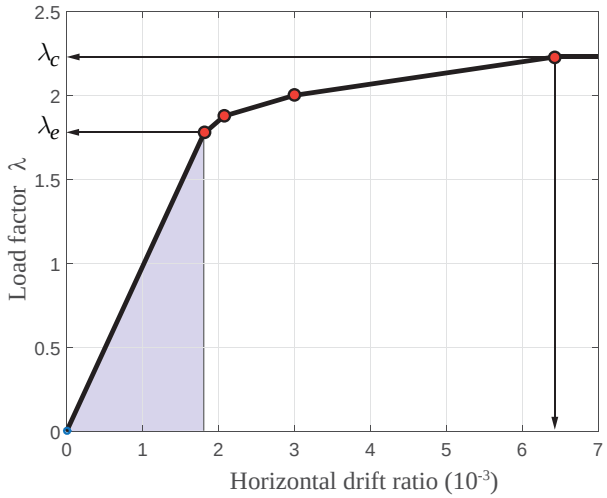

Fig. 4.15: Piecewise linear response of portal frame under increasing load factor λ to incipient collapse

Fig. 4.15 shows the piece-wise linear response of the portal frame with linear elastic, perfectly-plastic element response under an increasing load factor λ from the unstressed state to incipient collapse. The load factor λ_e at the first hinge to form is approximately 1.8, the next hinge forms at a load factor of approximately 1.9, the third hinge at a load factor of approximately 2, and the last hinge that converts the structure to a collapse mechanism forms at the load factor $\lambda_c = 2.229$. The load factor-horizontal drift ratio pairs at each hinge formation are marked with a red marker, but are also clear from the abrupt change of the slope of the relation between load factor and horizontal drift.

For the problem in hand both the vertical and the horizontal force are multiplied by the load factor λ. In practical applications for multi-story frames the vertical forces representing gravity effects remain

constant while the horizontal forces are incremented to collapse. This incremental response analysis is known as *push-over analysis*.

4.3.5 Conclusions

1) A linear elastic analysis of a structure gives the displacements, internal forces and support reactions up to the point of the most highly stressed element reaching the plastic capacity.
2) The upper and lower bound theorem of plastic analysis gives the collapse load factor λ_c of a structure under a given reference load $\boldsymbol{P}_{ref}$. For a complete collapse mode a unique solution for the basic forces is available from the equilibrium equations. For a partial collapse mode the unique determination of the basic forces is possible with the force and displacement method of analysis.
3) Once a unique solution for the basic forces $\boldsymbol{Q}_c$ at incipient collapse is available it is possible to determine the displacements and deformations at incipient collapse for linear elastic-perfectly plastic element response.
4) With the collapse mechanism kinematics we can determine the free global dof displacements and plastic deformations at any point past the initiation of the collapse mechanism.